

Numerical solutions for flow in porous media

J.G. Wang^{1,*†}, C.F. Leung² and Y.K. Chow²

¹*Tropical Marine Science Institute, National University of Singapore, Singapore 119260, Singapore*

²*Department of Civil Engineering, National University of Singapore, Singapore 119260, Singapore*

SUMMARY

A numerical approach is proposed to model the flow in porous media using homogenization theory. The proposed concept involves the analyses of micro-true flow at pore-level and macro-seepage flow at macro-level. Macro-seepage and microscopic characteristic flow equations are first derived from the Navier–Stokes equation at low Reynolds number through a two-scale homogenization method. This homogenization method adopts an asymptotic expansion of velocity and pressure through the micro-structures of porous media. A slightly compressible condition is introduced to express the characteristic flow through only characteristic velocity. This characteristic flow is then numerically solved using a penalty FEM scheme. Reduced integration technique is introduced for the volumetric term to avoid mesh locking. Finally, the numerical model is examined using two sets of permeability test data on clay and one set of permeability test data on sand. The numerical predictions agree well with the experimental data if constraint water film is considered for clay and two-dimensional cross-connection effect is included for sand. Copyright © 2003 John Wiley & Sons, Ltd.

KEY WORDS: homogenization method; characteristic flow; penalty method; permeability; constraint water film; two-dimensional effect; anisotropy

1. INTRODUCTION

Problems involving seepage in porous media are important in many fields [1–7]. These include seepage and consolidation problems in land reclamation [1] and underground waste disposal in geotechnical engineering [2], filter problems in chemical engineering [3, 10], and bio-fluid flow in bioengineering of human body [4]. Macro-analyses are generally carried out to tackle the average pore water pressure and velocity in porous medium [5]. However, macro-analysis has two major disadvantages. Firstly, it can only obtain the macro-pseudo velocity and pore water pressure within the entire porous media. The true velocity and pore water pressure at pore level is difficult or impossible to determine. In geotechnical engineering, the true velocity at pore level is an important factor in the design of filter that protects the sand from boiling and piping [6, 7].

*Correspondence to: J.G. Wang, Tropical Marine Science Institute, National University of Singapore, Singapore 119260, Singapore

†E-mail: tmswjg@nus.edu.sg

Contract/grant sponsors: National University of Singapore; contract/grant number RP3940674 Contract/grant sponsors: National Science and Technology Board of Singapore

Secondly, macro-analysis typically employs the coefficient of permeability in Darcy's law to express the micro-structure effect of porous medium on micro-hydraulic flow resistance [8, 9].

Many studies have been carried out to investigate the effect of micro-structures on flow in porous media [2, 3, 6–11]. For example, Kim *et al.* [11] studied Darcy's law within a representative volume element (RVE) through volume averaging theorem. A closed-form of Darcy's law was developed from the interaction of pore water and solid particles. Their method still has two issues remaining to be solved. The first is the relationship between the complicated micro-structures of porous media and the coefficient of permeability. In particular, the boundary condition for the RVE is not clear if the computation at micro-scale level is carried out. The second is that both macro-scale problem and micro-scale problem are not clearly defined [10]. In the 1970s, a two-scale homogenization theory was developed based on asymptotic expansions [8]. The homogenization theory can consider the behaviours simultaneously at both macro- and micro-scale levels. The first important result using homogenization theory was obtained by Sanchez-Palencia in 1974 on flow through porous media [8]. Since then, most researches focused on a formal expansion of Navier–Stokes equation, for example in Reference [12]. Numerical approaches are also proposed [13, 14]. Lee *et al.* [14] proposed a mixed mode of pressure and velocity for a solute transfer and dispersivity problem. Numerical methods for homogenization theory are successful in composite materials because their micro-structures are designed and determined. However, the situation in geotechnical engineering is a little different. This is because the micro-structure of soil masses is usually unknown and only index such as void ratio or weight fraction [15] can be measured. Some schemes such as Sierpinski carpets [13] or well-random media [16] were proposed to partially solve this problem in computation. However, these models are not capable of handling variable soil conditions. In this paper, the concept of equivalent particle size, which can be determined experimentally, is proposed to join tackle the computation for a variety of soil conditions.

The mixed mode of velocity and pressure for incompressible Navier–Stokes equation has its limitation. For example, the zero divergence condition of velocity field will produce a discrete algebraic system equation with zero diagonal terms if Galerkin's formulation is used. This limitation of mixed mode can be circumvented by the penalty method as only velocities are included in the weak form. The number of unknowns is largely reduced [17], too. One drawback for the penalty method is the ill-conditioning of the system matrix if penalty parameter is not appropriately selected. When penalty parameter is sufficiently large, the integration for volumetric term should be carefully treated. Otherwise, mesh locking may occur for some meshes. The reduced integration approach [18] can avoid mesh locking. In the authors' knowledge, the penalty method has not been applied to the characteristic function of fluid flow in porous media.

This paper proposes a numerical approach to model the flow of porous media from micro-analysis. The coefficient of permeability of clay and sand is numerically computed. This numerical approach is based on the two-scale asymptotic analysis of fluid channels in porous media. It is capable of handling micro-true flow analysis at pore-level and macro-seepage analysis simultaneously. This is useful to understand the behaviours of seepage at both macro- and micro-scale levels. As a preliminary, pore wall is assumed to be rigid in this paper. The characteristic equation at micro-scale level is numerically solved through a penalty method and reduced integration scheme. In order to carry out the computation in micro-scale level, an equivalent particle size was introduced into the unit cell. This largely simplifies the complicated

micro-structures of porous media and makes the computation applicable in practice. As the equivalent particle size is determined from a pair of macro-scale experimental data, the geometry of the pores is partially expressed by the equivalent particle. Using this numerical approach, the micro-structural effects such as constraint water film in clay and multi-dimensional effect in sand are studied. The numerical predictions are compared with experimental data.

This paper is organized as follows. Firstly, the micro-fluid flow is described through Navier–Stokes equation at low Reynolds number along micro-pore channels. A two-scale homogenization theory based on asymptotic expansion is introduced to derive the macro-seepage equation and microscopic characteristic equation. The similarity between the Stokes flow and the characteristic flow is discussed. This similarity is helpful to construct the solution structures of the characteristic flow from the known solution of Stokes flow. Secondly, a penalty finite element approach is developed for the solution of the characteristic equation for incompressible flow. Reduced integration is adopted for the volumetric term in order to avoid mesh locking. Thirdly, the proposed numerical model is verified by the comparison of the permeability of two sets of experimental data on clay and one set of experimental data on sand. The effects of constraint water film for clay and two-dimensional cross-connection for sand are investigated and finally, concluded.

2. MICRO-CHANNEL FLUID FLOW IN POROUS MEDIA

Micro-channel fluid flow in porous media is usually assumed to follow the Navier–Stokes flow for low Reynolds number. However, boundary conditions for such a problem are complicated. For the micro-channel fluid flow, the governing equation and boundary conditions can be generally expressed as follows:

Equation of motion

$$-\frac{\partial P}{\partial x_i} + \mu \frac{\partial^2 V_i}{\partial x_i \partial x_j} + \rho X_i = 0 \tag{1}$$

Continuity equation (incompressible case)

$$\frac{\partial V_i}{\partial x_i} = 0 \tag{2}$$

Boundary conditions

$$V_i = 0 \quad \text{on } \Gamma$$

$$V_i = \bar{V}_i \quad \text{on } \Gamma_F$$

or

$$P = \bar{P} \quad \text{on } \Gamma_F \tag{3}$$

where V_i is the true velocity in the pore channel of porous media, P the pore water pressure, μ the coefficient of viscosity, ρ the density of water, ρX_i the unit body force, Γ the fluid–solid interface, and x_i is the i th component of co-ordinates. \bar{V}_i and \bar{P} are the prescribed velocity and pressure on fluid external boundary, Γ_F , respectively. Index i is a free index and index j is a

dummy index that denotes the summation. For two-dimensional flow $i, j = 1, 2$ and for three-dimensional flow $i, j = 1, 2, 3$.

An exact solution is normally required to evaluate the above equations along all pore channels in the porous media. This requires huge computation time because of complexity of micro-channels. An approximation of the true fluid flow should include the main properties of fluid flow in porous media at both macro- and micro-levels. Homogenization theory based on asymptotic expansions is an appropriate tool to describe the two-scale properties simultaneously. In the homogenization approach, a local problem at micro-scale describes the micro-characteristic flow, and a macro-seepage problem at macro-scale analyses the average pore pressure and velocity. The micro- and macro-flows are linked through the homogenized coefficients of permeability.

3. ASYMPTOTIC EXPANSION

3.1. Periodic expansion with scale parameter

Figure 1 expresses a typical porous medium domain of flow. The micro-channels are complicated and simplified one-dimensional (1D) or two-dimensional (2D) unit cells can be regarded as the fundamental cells. A scale parameter ε is employed to link the unit cell and whole flow domain:

$$\mathbf{y} = \frac{\mathbf{x}}{\varepsilon} \quad (4)$$

where \mathbf{x} are global co-ordinates and \mathbf{y} local co-ordinates. True variables such as velocity and pressure are hence functions of ε , denoted as $V_i^\varepsilon(\mathbf{x})$ and $P^\varepsilon(\mathbf{x})$. They can be expressed with following asymptotic expansions:

$$\begin{aligned} V_i^\varepsilon(\mathbf{x}) &= \varepsilon^2 V_i^0(\mathbf{x}, \mathbf{y}) + \varepsilon^3 V_i^1(\mathbf{x}, \mathbf{y}) + \dots \\ P^\varepsilon(\mathbf{x}) &= P^0(\mathbf{x}, \mathbf{y}) + \varepsilon P^1(\mathbf{x}, \mathbf{y}) + \dots \end{aligned} \quad (5)$$

The $V_i^\alpha(\mathbf{x}, \mathbf{y})$ and $P_i^\alpha(\mathbf{x}, \mathbf{y})$ ($\alpha = 0, 1, 2, \dots$) are functions of global co-ordinates \mathbf{x} and local co-ordinates \mathbf{y} . The \mathbf{Y} -periodicity is expressed as

$$\begin{aligned} P^\varepsilon(\mathbf{x}, \mathbf{y}) &= P^\varepsilon(\mathbf{x}, \mathbf{y} + \mathbf{Y}) \\ V_i^\alpha(\mathbf{x}, \mathbf{y}) &= V_i^\alpha(\mathbf{x}, \mathbf{y} + \mathbf{Y}) \end{aligned} \quad (6)$$

Body force of fluid is expressed using the same expansion:

$$X_i^\varepsilon(\mathbf{x}) = X_i^0(\mathbf{x}) + \varepsilon^1 X_i^1(\mathbf{x}, \mathbf{y}) + \varepsilon^2 X_i^2(\mathbf{x}, \mathbf{y}) + \dots \quad (7)$$

Mathematical chain rules for scale parameter ε are as

$$\frac{\partial}{\partial x_i} \Rightarrow \frac{\partial}{\partial x_i} + \frac{\partial}{\partial y_k} \frac{\partial y_k}{\partial x_i} = \frac{\partial}{\partial x_i} + \frac{1}{\varepsilon} \frac{\partial}{\partial y_i} \quad (8)$$

for the first-rank derivatives and

$$\frac{\partial^2}{\partial x_i \partial x_i} \Rightarrow \frac{\partial^2}{\partial x_i \partial x_i} + \frac{2}{\varepsilon} \frac{\partial^2}{\partial x_i \partial y_i} + \frac{1}{\varepsilon^2} \frac{\partial^2}{\partial y_i \partial y_i} \quad (9)$$

for the second-rank derivatives.

The motion equation in Equation (1) is discussed. A ε -series polynomial is obtained from Equation (5) to (9). This polynomial can be expressed in the following form:

$$\sum_{\alpha=-1}^{\infty} (\cdot) \varepsilon^\alpha = 0 \tag{10}$$

Equation (10) should be held for any ε , which implies that the coefficients denoted by ‘ \cdot ’ are zeros for all order ε . The coefficients at different orders ε express different physical meanings. For example, the coefficient for the ε^{-1} -term is

$$\frac{\partial P^0}{\partial y_i} = 0 \quad \text{in } Y_F \tag{11}$$

where Y_F is the fluid domain in a unit cell. Equations (11) implies that $P^0(\mathbf{x}, \mathbf{y}) = P^0(\mathbf{x})$. In another word, the zero-order pore pressure is independent of local co-ordinates \mathbf{y} . This result is of special importance because $P^0(\mathbf{x})$ is the leading term of pore water pressure. This suggests that the homogenization method be applicable for this case.

A recursive relation is developed through the coefficient of ε^0 -term. The governing equation for the higher-order pore water pressure P^1 is obtained as

$$-\frac{\partial P^0}{\partial x_i} - \frac{\partial P^1}{\partial y_i} + \mu \frac{\partial^2 V_i^0}{\partial y_k \partial y_k} + \rho X_i^0 = 0 \quad \text{in } Y_F \tag{12}$$

The same expansion is applied to the continuity equation given by Equation (2):

$$\varepsilon \frac{\partial V_i^0}{\partial y_i} + \varepsilon^2 \left[\frac{\partial V_i^0}{\partial x_i} + \frac{\partial V_i^1}{\partial y_i} \right] + \dots = 0 \quad \text{in } Y_F \tag{13}$$

This expansion is held for any scale parameter ε . For the ε^1 -term, incompressible condition is again obtained at micro-level as follows:

$$\frac{\partial V_i^0}{\partial y_i} = 0 \quad \text{in } Y_F \tag{14}$$

The recursive formula is obtained from the ε^2 -term:

$$\frac{\partial V_i^0}{\partial x_i} + \frac{\partial V_i^1}{\partial y_i} = 0 \quad \text{in } Y_F \tag{15}$$

The boundary condition at the fluid–solid interface, Γ , can be also expanded as follows:

$$\varepsilon^2 V_i^0 + \varepsilon^3 V_i^1 + \dots = 0 \quad \text{on } \Gamma \tag{16}$$

The above equation is decomposed into

$$V_i^0 = 0, \quad V_i^1 = 0, \dots \text{ on } \Gamma \tag{17}$$

The $(\partial P^0 / \partial x_k - \rho X_k^0)(k = 1, 2, 3)$ is a function in terms of \mathbf{x} co-ordinates only. The two-scale co-ordinates are separated as follows:

$$\begin{aligned} V_i^0 &= - \left(\frac{\partial P^0}{\partial x_k} - \rho X_k^0 \right) v_i^k \\ P^1 &= - \left(\frac{\partial P^0}{\partial x_k} - \rho X_k^0 \right) p^k \\ &(k = 1, 2, 3) \end{aligned} \quad (18)$$

where v_i^k and p^k are the characteristic functions of velocity and pressure, respectively. Normalization of the equations denoted by Equations (12) and (14) yields a characteristic equation for unit cell as well as no-slip and periodic conditions. This characteristic equation is termed as a local problem. The average equation over whole unit cell domain is called a macro-seepage problem.

3.2. Local problem

Equation of motion

$$-\frac{\partial p^k}{\partial y_i} + \mu \frac{\partial^2 v_i^k}{\partial y_j \partial y_j} + \delta_{ik} = 0 \quad (k = 1, 2, 3) \quad (19)$$

Continuity equation (incompressible case)

$$\frac{\partial v_i^k}{\partial y_i} = 0 \quad (k = 1, 2, 3) \quad (20)$$

Boundary conditions

$$\begin{aligned} v_i^k &= 0 && \text{on } \Gamma \\ \left. \begin{aligned} p^k(\mathbf{x}, \mathbf{y}) &= p^k(\mathbf{x}, \mathbf{y} + \mathbf{Y}) \\ v_i^k(\mathbf{x}, \mathbf{y}) &= v_i^k(\mathbf{x}, \mathbf{y} + \mathbf{Y}) \end{aligned} \right\} && \text{periodicity condition on } \Gamma_F \end{aligned} \quad (21)$$

It is helpful to compare above governing equations and boundary conditions of v_i^k with the Navier–Stokes equations for velocity V_i .

(1) Navier–Stokes flow expressed by Equation (1) has true body force, while characteristic flow expressed by Equation (19) has characteristic body force $\{\delta_{ik}\}$. This characteristic body force is not a physical force. It exists only for micro-characteristic flow when the macro-flow is along that direction. Therefore, the characteristic body force is also termed as pseudo-body force.

(2) Incompressible condition is true for both characteristic flow and Navier–Stokes flow. The fluid at micro-scale is still incompressible.

(3) Both flows have no-slip boundary condition along the fluid–solid interface Γ . This is the physical description for the no-slip condition at both macro- and micro-scale levels.

(4) However, boundary conditions are different on the fluid boundary Γ_F . The Navier–Stokes flow gives velocity \vec{V}_i , pressure \bar{P} or shear stress (a mixed boundary), while the characteristic flow requires only periodicity on the artificial fluid boundary Γ_F .

Therefore, both flows should have similar structure of solutions. This similarity of solution structures provides a clue to pursue an analytical or numerical solution of characteristic flow from the solution of Navier–Stokes flow.

3.3. Macro-problem–Seepage equation

At macro-scale, the main concern is to obtain the average velocity or pore water pressure in a unit cell. The well-known Darcy’s law can be obtained through a volume averaging of true velocity in a unit cell, \tilde{V}_i^0 . Particularly, the averaging of Equation (18) is given as

$$\tilde{V}_i^0 = \frac{1}{|Y|} \int_{Y_F} V_i^0 \, dV = K_{ij} \left(\rho X_j^0 - \frac{\partial P^0}{\partial x_j} \right) \tag{22}$$

where the permeability tensor, K_{ij} , is the volume average of characteristic velocity given as

$$K_{ij} = \frac{1}{|Y|} \int_{Y_F} v_i^j \, dV \tag{23}$$

where $|Y|$ is the volume of the unit cell which includes the fraction of solid matrix. The permeability of porous media is a macro-tensor. It is completely computed from the micro-flow velocity, v_i^j , in terms of volume averaging or porosity of the porous media. Equation (23) is therefore a linkage between macro- and micro-analyses. The macro-seepage problem is obtained through an average procedure of the continuity equation of Equation (15):

$$\frac{\partial}{\partial x_i} \left\{ K_{ij} \left(\frac{\partial P^0}{\partial x_j} - \rho X_j^0 \right) \right\} = 0 \tag{24}$$

The permeability tensor can be determined analytically through characteristic flow within micro-fluid channels. The key issue for the characteristic flow is how to compute the characteristic function v_i^j . A numerical procedure based on penalty finite element method is proposed.

4. WEAK FORMS OF LOCAL PROBLEM AND ITS DISCRETIZATION

4.1. Weak forms of local problem

A bulk modulus λ is introduced to replaces the original incompressible condition with a slightly compressible condition as follows:

$$\frac{\partial v_i^k}{\partial y_i} + \frac{p^k}{\lambda} = 0 \tag{25}$$

If λ is big enough, the approximation is sufficiently accurate. For example, when $\lambda \rightarrow +\infty$, $p^k/\lambda \rightarrow 0$. Using Equation (25), the equation of motion Equation (19) can be expressed as

$$\lambda \frac{\partial^2 v_j^k}{\partial y_i \partial y_j} + \mu \frac{\partial^2 v_i^k}{\partial y_j \partial y_j} + \delta_{ik} = 0 \tag{26}$$

Equation (26) significantly reduces the complexity of the computation procedure because only characteristic velocity is included. Its weak form is obtained by applying a weight function δv_i

($\delta v_i = 0$ on Γ) that only varies with the fast variable \mathbf{y} and is the \mathbf{Y} -periodicity, $\delta v_i(\mathbf{y}) = \delta v_i \times (\mathbf{y} + \mathbf{Y})$.

$$\int_{Y_F} \left(\lambda \frac{\partial^2 v_j^k}{\partial y_i \partial y_j} + \mu \frac{\partial^2 v_i^k}{\partial y_j \partial y_j} \right) \delta v_i \, dV = - \int_{Y_F} \delta v_i \delta_{ik} \, dV \quad (27)$$

By applying the Green–Gauss theorem to the second term at the left-hand side, one gets

$$\int_{Y_F} \mu \frac{\partial^2 v_i^k}{\partial y_j \partial y_j} \delta v_i \, dV = \oint_{\partial Y_F} \mu \frac{\partial v_i^k}{\partial y_j} n_j \delta v_i \, ds - \int_{Y_F} \mu \frac{\partial v_i^k}{\partial y_j} \frac{\partial(\delta v_i)}{\partial y_j} \, dV \quad (28)$$

The boundary term is zero because

$$\oint_{\partial Y_F} \mu \frac{\partial v_i^k}{\partial y_j} n_j \delta v_i \, ds = \int_{\Gamma} \mu \frac{\partial v_i^k}{\partial y_j} n_j \delta v_i \, ds + \int_{\Gamma_F} \mu \frac{\partial v_i^k}{\partial y_j} n_j \delta v_i \, ds \quad (29)$$

Since the first term vanishes due to no-slip condition ($\delta v_i = 0$ on Γ), and the second term vanishes due to periodicity on fluid boundary Γ_F . Similarly, the first term of Equation (27) becomes as

$$\int_{Y_F} \lambda \frac{\partial^2 v_j^k}{\partial y_i \partial y_j} \delta v_i \, dV = \oint_{\partial Y_F} \lambda \frac{\partial v_j^k}{\partial y_j} n_i \delta v_i \, ds - \int_{Y_F} \lambda \frac{\partial v_j^k}{\partial y_j} \frac{\partial(\delta v_i)}{\partial y_i} \, dV = - \int_{Y_F} \lambda \frac{\partial v_j^k}{\partial y_j} \frac{\partial(\delta v_i)}{\partial y_i} \, dV \quad (30)$$

Thus, the weak form of Equation (26) is finally expressed as

$$\int_{Y_F} \lambda \frac{\partial v_j^k}{\partial y_j} \frac{\partial(\delta v_i)}{\partial y_i} \, dV + \int_{Y_F} \mu \frac{\partial v_i^k}{\partial y_j} \frac{\partial(\delta v_i)}{\partial y_j} \, dV - \int_{Y_F} \delta v_k \, dV = 0 \quad (31)$$

This is a weak form of the local problem with penalty method. When the bulk modulus λ (as penalty parameter) is determined, the characteristic velocity v_i^k can be uniquely solved.

4.2. Discretization of characteristic velocity

Fluid domain Y_F is divided into n sub-domains, whose sub-domain Y_s is an element. Each element has m nodes. The characteristic velocity in an element is approximated in terms of the nodal characteristic velocity V_{ij}^k and shape function Φ_j :

$$v_i^k \cong \sum_{j=1}^m V_{ij}^k \Phi_j \quad (32)$$

The weight function is approximated using the same shape function:

$$\delta v_i \cong \sum_{j=1}^m \delta V_{ij} \Phi_j \quad (33)$$

where δV_{ij} is the weight function at the j th node.

Equation (31) can be discretized into

$$(\mathbf{K}^V + \mathbf{K}^{VP}) \mathbf{V}^k = \mathbf{F}^k \quad (k = 1, 2, 3) \quad (34)$$

where the stiffness matrix associated with shear part is

$$K_{rs}^V = \int_{Y_s} \mu \frac{\partial \Phi_r}{\partial y_j} \frac{\partial \Phi_s}{\partial y_j} \, dV \quad (35)$$

and the stiffness matrix associated with volume part is

$$K_{rs}^{vp} = \int_{Y_s} \lambda \frac{\partial \Phi_r}{\partial y_i} \frac{\partial \Phi_s}{\partial y_j} dV \tag{36}$$

The characteristic loading induced by characteristic body force is

$$F_{si}^k = \delta_{ik} \int_{Y_s} \Phi_s dV \tag{37}$$

Special care should be taken for the numerical integrations of \mathbf{K}^V and \mathbf{K}^{VP} . Otherwise, mesh locking will take place for non-triangle elements. In this paper, the reduced integration procedure [18] is used for stiffness \mathbf{K}^{VP} , while normal integration is applied to stiffness \mathbf{K}^V .

5. NUMERICAL PROCEDURES AND EXAMPLES

The micro-structures of porous media are complex. This paper simplifies these micro-structures into 1D flow and 2D flow models as shown in Figure 1. With these models, the effect of bulk modulus is studied. This numerical method is then applied to study the permeability of clay and artificial sand. For clay, the effect of constraint water film around particles is studied in detail.

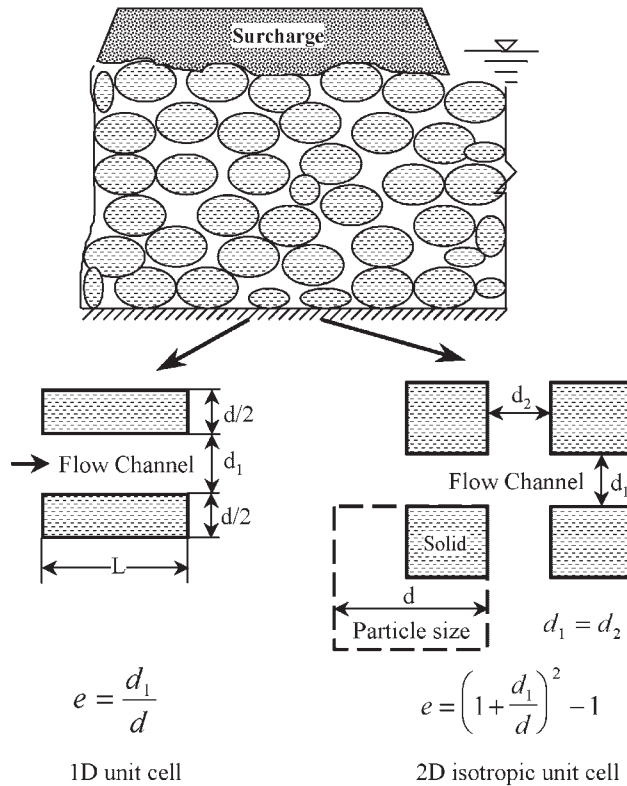


Figure 1. Seepage through porous media.

For sand, multi-dimensional effect is studied by comparing 1D results with 2D results. Finally, anisotropic flow is numerically analysed.

5.1. Numerical procedure and computational parameter

Isoparametric elements with 8-nodes are used in computations. Shear stiffness, \mathbf{K}^V , is numerically treated by 3×3 point Gaussian integration, while volumetric stiffness, \mathbf{K}^{VP} , is numerically treated by 2×2 point Gaussian integration. No-slip condition is imposed on fluid–solid boundaries. In addition, periodic condition is applied on artificial fluid–fluid boundaries Γ_F . Material parameter includes water viscosity $\mu/\rho g = 1.2 \times 10^{-2}$ cm s at 15°C . Figure 2 shows the effect of penalty parameter (bulk modulus) λ on the coefficient of permeability for one-dimensional flow. Two-dimensional isotropic flow yields similar results. When λ is small, the error of numerical results is big. However, numerical results approach to a stable value when $\lambda \geq 10$. Figure 3 shows 1D and 2D flow patterns when $\lambda = 10$. These results indicate that the proposed numerical procedure is reasonable as long as λ is larger than 10. Hence in subsequent computations, the penalty parameter is taken as 10.

5.2. Permeability of clay and constraint water film effect

5.2.1. *Equivalent particle size.* In the first example, the coefficient of the permeability of clay is studied using the experimental data from Casteleiro [19] who had carried out seven types of experiments to determine the coefficient of permeability of dredged clay. These experiments

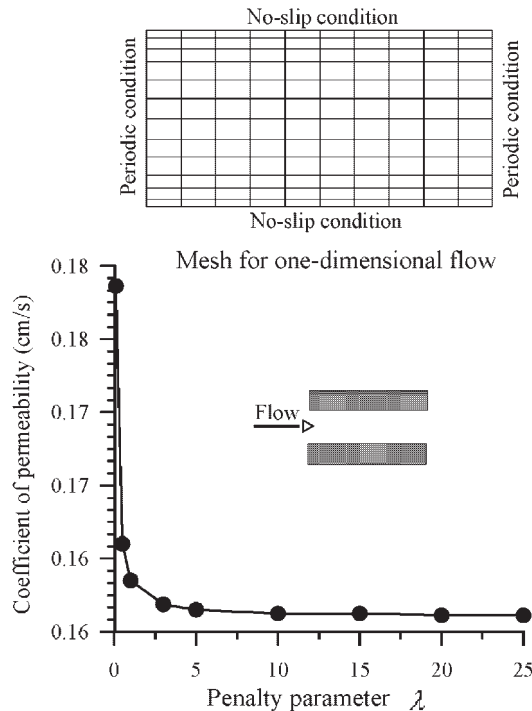
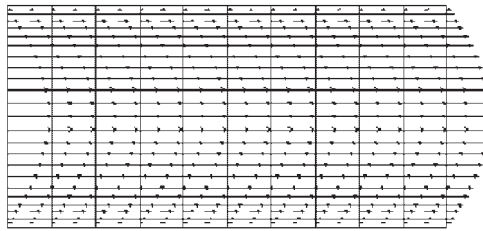
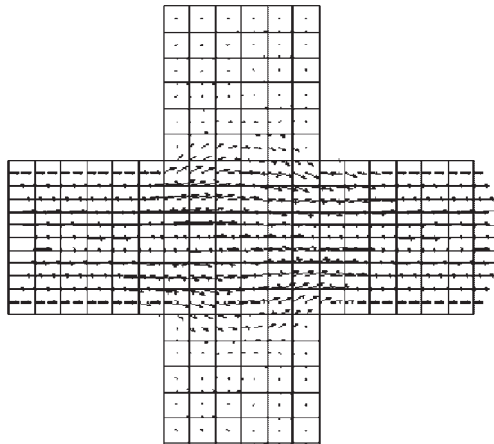


Figure 2. Effect of penalty parameter on permeability.



Characteristic flow vector for one-dimensional flow



Characteristic flow vector for two-dimensional flow

Figure 3. Flow patterns for 1D and 2D flows.

include conventional consolidation, single load consolidation, slurry consolidation, direct permeability, gravity drainage, vacuum drainage, and field infiltration tests. Figure 4 plots the coefficients of permeability against void ratio, e , of the dredged clay.

A micro-structural model termed unit cell is necessary to compute the micro-flow and the coefficient of the permeability for a given void ratio using the proposed numerical approach. The 1D unit cell shown in Figure 1 has two important geometrical parameters: equivalent particle size d and void ratio e . The coefficient of the permeability is generally expressed as

$$k = f(d, e, \mu) \tag{38}$$

As the coefficient of viscosity is a constant at a given temperature, the equivalent particle size can be back calculated through a single experimental data of (k, e) . For this model, a typical experimental data is taken as $(k, e) = (1.565 \times 10^{-8} \text{ m/s}, 3.5115)$. The equivalent particle size is determined to be $7.66 \times 10^{-5} \text{ cm}$ based on this set of data. Using the equivalent particle size, the coefficient of the permeability can be computed for various void ratios. The numerical results are represented by thick solid line in Figure 4. Similarly, 2D isotropic unit cell model as shown in Figure 1 is also used to predict the coefficient of the permeability. It is found that the 2D

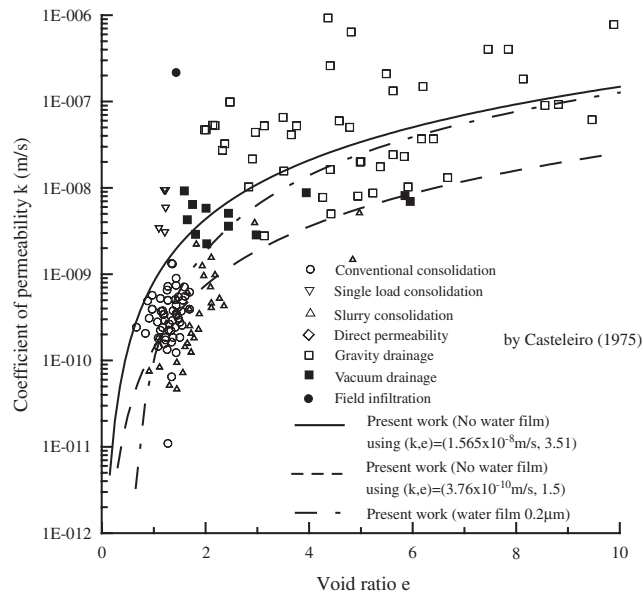


Figure 4. Comparison of numerical predictions with Casteleiro's experimental data.

results are slightly lower than the 1D ones. Thus multi-dimensional effect is insignificant for this clay.

Numerical results agree reasonably well with experimental data for the clay with void ratio larger than 3. However, numerical predictions are higher than experimental data for the clay with void ratio smaller than 3. We take another set of $(k, e) = (3.76 \times 10^{-10} \text{ m/s}, 1.5)$ to reanalyse the model. This new pair of experimental data roughly represents the mean of conventional consolidation tests (majority of these test data have void ratio less than 3). The dash line as shown in Figure 4 is the numerical predictions. Although the model predicts reasonably well for void ratio smaller than 3, it clearly under-predicts the permeability with larger void ratio. Equivalent particle can include some range of void ratios; however, it cannot cover whole void ratios. These discrepancies may be due to the effect of constraint water film.

5.2.2. Effect of constraint water film. Constraint water film refers to the adhesive water film around a particle. This water film is of special importance to the materials with small particles such as clay, because it forms a typical two-layer micro-structure [20]. As established earlier, one-dimensional flow applies for clay. The effect of constraint water film is simulated by a distribution of coefficient of viscosity along normal direction as shown in Figure 5. This distribution is contrast to a constant viscosity all flow channels. The viscosity coefficient increases considerably within some distance from its partial surface. The water film narrows flow channels, thus reducing the permeability of clay. The reduction ratio depends on pore sizes. The smaller the pore size is, the larger the reduction ratio of flow channels. For clay with the same particle size, smaller void ratio yields greater reduction. The measured void ratio of clay is not effective to free water passages. An effective void ratio is defined as that void ratio for free water passages. If the thickness of constraint water film is Δd , the effective void ratio e is then

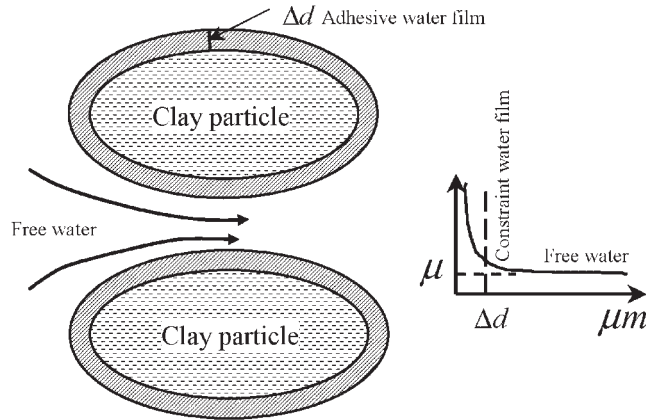


Figure 5. Double water film model.

determined by

$$e = \frac{d_1^0 - \Delta d}{d^0 + \Delta d} \tag{39}$$

and the equivalent particle size is

$$d = d^0 + \Delta d \tag{40}$$

where superscript ‘0’ refers to the state without water film ($\Delta d \equiv 0$). A simple closed-form solution is obtained for the coefficient of the permeability in one-dimensional flow:

$$k = \frac{\rho g (d_1^0 - \Delta d)^3}{3\mu (d^0 + d_1^0)} \tag{41}$$

where $(d^0 + d_1^0)$ is the characteristic size of a unit cell. When $d_1^0 - \Delta d \leq 0$, there is no flow passage and $k = 0$. This implies that a critical void ratio exists. When the actual void ratio is below this critical void ratio, the coefficient of the permeability is zero. At this time, constraint water film completely blocks flow channels.

The thickness of constraint water films varies with constituents of clay. Polubarinova-Kochina [20] found that the thickness should not exceed $0.5 \mu\text{m}$. A thickness of $0.2 \mu\text{m}$ water film is assumed in this example. The numerical predictions which include constraint water films are denoted by the dash dot line in Figure 4. The agreement is good between numerical and experimental k values for the entire range of void ratios. This shows that the effect of constraint water film plays an important role for clay with relatively small void ratio. Because the equivalent particle size of clay is small, the water film can block the flow passage heavily.

The permeability of remolded clays has been experimentally studied by Carrier and Beckman [21] who conducted stress-controlled and constant rate-of-deformation consolidometer tests. A total of 52 samples are represented, of which 22 are phosphatic, 13 are dredged materials, and 17 are remolded natural clays. Figure 6 compares the Carrier–Beckman’s experimental data with the numerical results with/without water film. The equivalent particle size is $5.7 \mu\text{m}$ from test point $(k, e) = (1.77 \times 10^{-8} \text{ m/s}, 5.0)$. The water film is taken to be $0.2 \mu\text{m}$ thick. In general, the numerical results agree reasonably well with experimental data. The effect of water film is only

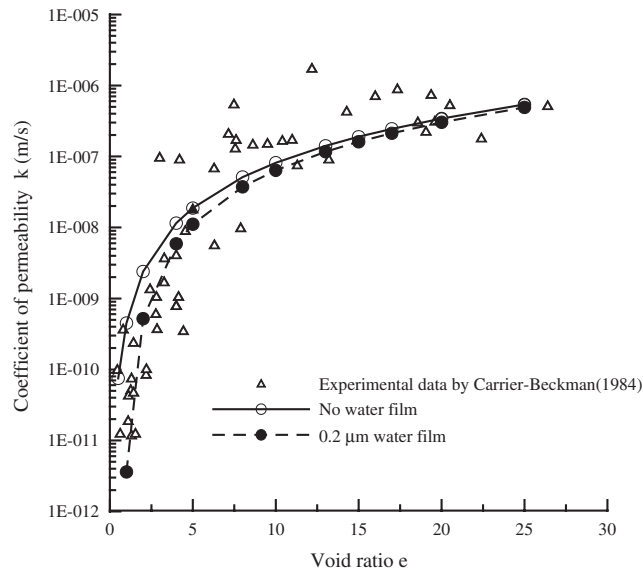


Figure 6. Comparison of numerical predictions with Carrier-Beckman's experimental data.

noticeable when the void ratio of clay is small. Numerical results using 2D isotropic unit cell model are close to 1D results. This confirms that 1D model is sufficient to predict the permeability of clay.

5.3. Permeability of sand and two-dimensional effect

Artificial uniform sand named as Wigner-Seitz grains was tested by Carman [22]. The equivalent particle size is to be 0.1135 cm if the data point $(k, e) = (4.694 \times 10^{-5} \text{ m/s}, 1.4437)$ is used. The experimental data are plotted in Figure 7. A small void ratio is taken so as to avoid possible multi-dimensional effect. The numerical results agree generally well with experimental data except for void ratio larger than 3. As sand has much bigger pore size than clay, the water film effect is not important. For sand, a major factor for this discrepancy may be from the multi-dimensional effect. This effect refers to the flow resistance at inter-connective pores. A conceptual 2D model is proposed to investigate the multi-dimensional effect.

The real flow channel in porous media is not always 1D. The zigzag channel flows interact with each other, thus increasing flow resistance. A simple 2D unit cell is conceived in Figure 1. Channels cross each other and their widths are d_1 and d_2 . Characteristic particle size is assumed to be d and d_1 is equal to d_2 for an isotropic flow. The void ratio e is

$$e = \left(1 + \frac{d_1}{d}\right)^2 - 1 \quad (42)$$

The coefficient of permeability can be determined if particle size and void ratio are known. This relation can be used to determine the equivalent particle size d if (k, e) is known. When d is known, the coefficient of the permeability can be determined for any void ratio. Figure 8 compares the distribution of characteristic velocity at void ratios $e = 0.331$ and 1.25,

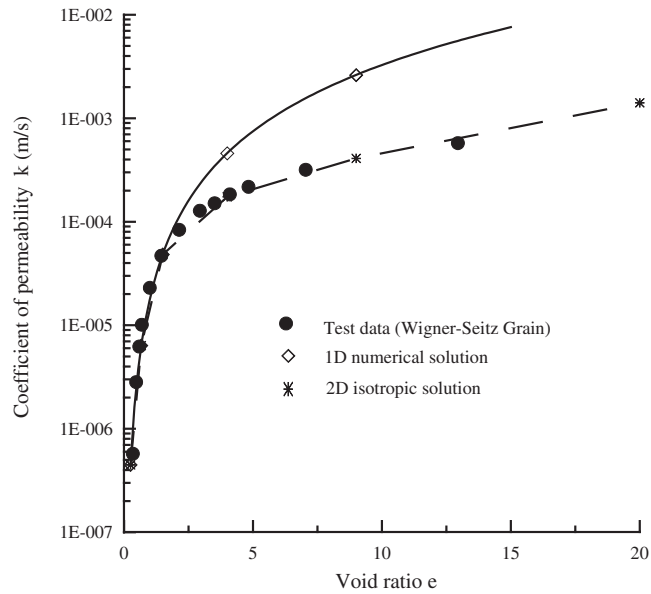


Figure 7. Comparison of numerical predictions with Wigner–Seitz grain experimental data.

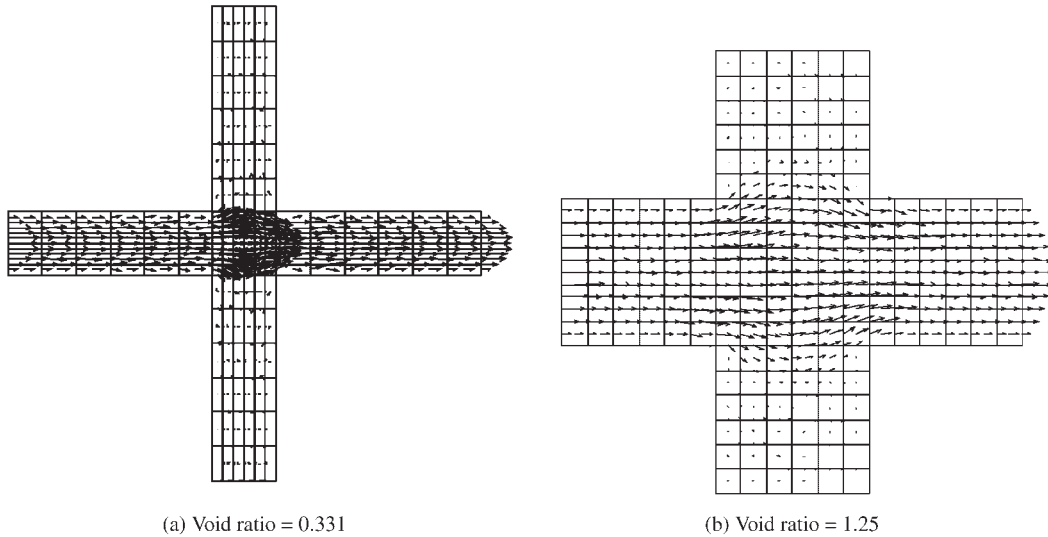


Figure 8. Cross-connection effect for different void ratios. (a) Void ratio = 0.331 and (b) void ratio = 1.25.

respectively. When the pore size is small, crossing effect is small and ignorable as illustrated in Figure 8(a). However, the effect cannot be ignored when pore sizes are big. For a bigger pore as shown in Figure 8(b), the cross-effect is significant and hence one-dimensional flow solution is not adequate to predict the coefficient of the permeability accurately. The numerical results

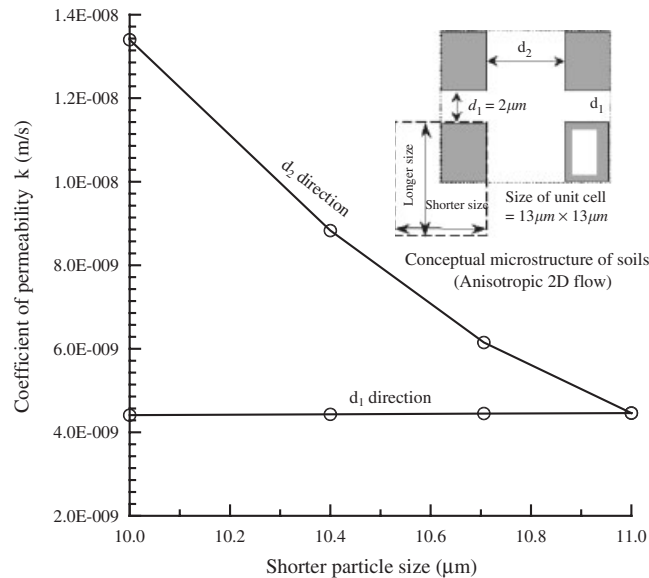


Figure 9. Anisotropic permeability due to anisotropic fluid channels.

with/without cross-effects are all plotted in Figure 7. It is evident that the 2D model is able to predict the coefficient of permeability for all void ratios. In summary, constraint water film affects the pore flow for small particles in small void ratio zone, while multi-dimensional effect affects the pore flow for big particles in large void ratio zone.

5.4. Effect of particle shape and anisotropic flow

Anisotropy of permeability is an important topic in practice. An anisotropic numerical model is shown in Figure 9. The model varies flow channel d_2 while keeping flow channel d_1 constant. Such a simulation is valid for clay as the shape of clay components is relatively flat [23]. A parameter study is carried out on a unit cell with $13 \mu\text{m} \times 13 \mu\text{m}$ in size. This unit cell represents a 2D isotropic flow with clay particles of $11 \mu\text{m}(d_1)$ by $11 \mu\text{m}(d_2)$ and flow channel of $2 \mu\text{m}$ wide. By varying d_2 and keeping d_1 , the numerical permeability along the d_1 and d_2 channels are shown in Figure 9. Two findings are made from the numerical results. Firstly, the coefficient of the permeability along d_1 channel is almost constant due to same pore size in this direction. This implies that the flow in this direction is hardly affected by the flow in other directions. Secondly, the coefficient of the permeability along d_2 channel increases with pore size d_2 . When pore sizes in both directions are the same, the permeability becomes identical. This is the case for isotropic flow. A limit case for $d_2 \rightarrow 0$ should be specially noted. For this limit case, the pore flow is only along d_1 channel. From the view of micro-analysis, an anisotropic flow is decomposed into two one-dimensional flows, as void ratio and characteristic particle size are all along that direction. In other words, one-dimensional numerical model is sufficient to describe a two-dimensional permeability if a directional porosity and a directional particle size are introduced into the present numerical model.

6. CONCLUSIONS

A numerical model for the flow in porous media is proposed and the coefficient of permeability is then computed. The characteristic equation at micro-level and seepage equation at macro-level are developed from a two-scale homogenization process of the Navier–Stokes flow in porous media. A penalty finite element approach is put forth to solve the characteristic equation at micro-level. The coefficients of permeability computed from the proposed approach are compared with experimental data for clays and sands. The effect of constraint water film is studied for clay while two-dimensional flow effect is studied for sands. Finally, anisotropy of permeability is discussed through the current numerical model. From these analyses, following conclusions can be drawn.

Macro-seepage equation and microscopic characteristic equation at low Reynolds number are obtained from the Navier–Stokes equation through a two-scale homogenization method. The Stokes flow and micro-level characteristic flow have some similarity in solution structures. This similarity indicates that characteristic flow is just a special case of Navier–Stokes flow. Their differences include body force and artificial boundary condition.

Penalty method is an efficient numerical approach in solving the characteristic equation if the penalty parameter adopted is sufficiently large. As only characteristic velocity is included in the weak form, penalty method minimizes unknowns in FEM. Reduced integration is applied to treat the volumetric integration in order to avoid mesh-locking for non-triangular element.

Constraint water film of clay has a vital effect on the coefficient of the permeability when the void ratio is small. However, the multi-dimensional effect can be ignored for clay because of small pore sizes. Constraint water film blocks flow channels and thus reduces the permeability of clay. Examples reveal that water film effect is significant when void ratio is less than 2. If the characteristic particle size of clay is taken as the particle size plus the thickness of constraint water film, one-dimensional model of unit cell is sufficiently accurate to predict the coefficient of permeability of clay.

Multi-dimensional effect becomes important for sand when void ratios are large as larger cross-channels produce greater resistance. On the other hand, constraint water film effect is established to be insignificant for sand.

NOMENCLATURE

d	equivalent particle size
e	void ratio
F_{si}^k	characteristic loading
K_{ij}	permeability tensor of porous media
K_{rs}^v	element shear stiffness matrix
K_{rs}^{vp}	element volume stiffness matrix
k	coefficient of permeability
m	nodal number in an element
n	element number
$P, P^e(\mathbf{x})$	pore water pressure
\bar{P}	pore water pressure at fluid boundary
$P^0(\mathbf{x})$	leading term of pore water pressure

PI	plastic index
PL	plastic limit
p^k	characteristic pressure
$V_i, V_i^e(\mathbf{x})$	true velocity
\tilde{V}_i	velocity at fluid boundary
\tilde{V}_i^0	macro-pseudo velocity of porous media flow
V_{ij}^k	Nodal characteristic velocity
v_i^k	characteristic velocity
\mathbf{x}	global co-ordinates
x_i	i th component of coordinates
ρX_i	unit body force
\mathbf{Y}	domain of a unit cell
\mathbf{y}	local co-ordinates
Y_F	fluid domain in a unit cell
Y_s	sub-domain or element domain
ε	scale parameter
μ	coefficient of viscosity
ρ	density of water
Γ	fluid–solid interface
Γ_F	fluid boundary or artificial fluid boundary
λ	bulk modulus or penalty parameter
δ_{ij}	characteristic body force or pseudo-body force
δv_i	weight function
δV_{ij}	weight function at the j th node.
Φ_j	shape function
Δd	thickness of the constraint water film

ACKNOWLEDGEMENTS

The funding for the research study is provided by research grant RP3940674 funded by the National University of Singapore and the National Science and Technology Board of Singapore.

REFERENCES

1. Wang JG, Leung CF, Chow YK. Consolidation analysis of lumpy fills using a homogenization method. *Proceedings of the 9th International Conference of the Association for Computer Method and Advances in Geomechanics*, Wuhan, China AA. Balkema Publisher: Rotterdam; Ed. by JX Yuan; 1075–1080.
2. Ichikawa Y, Kawamura K, Nakano M, Kitayama K, Kawamura H. Unified molecular dynamics and homogenization analysis for bentonite behaviour: current results and future possibilities. *Engineering Geology* 1999; **54**:21–31.
3. Lemaitre R, Adler PM. Fractal porous media IV: three-dimensional stokes flow through random media and regular fractals. *Transport in Porous Media* 1990; **5**:325–340.
4. Mow VC, Guo XE. Mechano-electrochemical properties of articular cartilage: their inhomogeneities and anisotropies. *Annu Review of Biomedical Engineering* 2002; **4**:175–209.
5. Singh P, Tewari K. Non-Darcy free convection from vertical surface in thermally stratified porous media. *International Journal of Engineering Science* 1993; **31**(9):1233–1242.
6. Yang T, Wang L. Microscale flow bifurcation and its macroscale implications in periodic porous media. *Computational Mechanics* 2000; **26**:520–527.
7. Auriault JL, Lewandowska J. One the cross-effects of coupled macroscopic transport equations in porous media. *Transport in Porous Media* 1994; **16**:31–52.

8. Sanchez-Palencia E. *Non-Homogeneous Media and Vibration Theory*, Lecture Notes in Physics, Vol. 127. Springer, Berlin, 1980.
9. Chen Z, Lyons SL, Qin G. Derivation of the Forchheimer law via homogenization. *Transport in Porous Media* 2001; **44**:325–335.
10. Whitaker S. *The Method of Volume Averaging*. Kluwer Academic Publishers: Dordrecht, 1999.
11. Kim JH, Ochoa JA, Whitaker S. Diffusion in anisotropic porous media. *Transport in Porous Media* 1987; **2**:327–356.
12. Auriault JL, Boutin C. Deformable porous media with double porosity. Quasi-statics, I: coupling effects. *Transport in Porous Media* 1992; **7**:63–82.
13. Adler PM. Fractal porous media III: transversal Stokes flow through random and Sierpinski carpets. *Transport in Porous Media* 1988; **3**:185–198.
14. Lee CK, Sun CC, Mei CC. Computation of permeability and dispersivities of solute or heat in periodic porous media. *International Journal of Heat Mass Transfer* 1996; **39**(4):661–676.
15. Wang JG, Leung CF, Ichikawa Y. A simplified homogenization method for mixed soils. *Computers and Geotechnics* 2002; **29**(6):477–500.
16. Sab K. On the homogenization and the simulation of random materials. *European Journal Mechanics A/Solids* 1992; **11**(5):585–607.
17. Codina R. An iterative penalty method for the finite element solution of the stationary Navier–Stokes equations. *Computer Methods in the Applied Mechanics and Engineering* 1993; **110**(3–4):237–262.
18. Hughes TJR. *The Finite Element Method—Linear Static and Dynamic Finite Element Analysis*. Prentice-Hall; Englewood Cliffs, NJ, 1987.
19. Casteleiro M. Mathematical model of one-dimensional consolidation and desiccation of dredged materials. *Ph.D. dissertation*, Northwestern University, 1975, USA.
20. Polubarinova-Kochina PYA. *Theory of Ground Water Movement*, Princeton University Press: Princeton, NJ, 1962.
21. Carrier WD, Beckman JF. Correlations between index tests and the properties of remolded clays. *Geotechnique* 1984; **34**(2):211–228.
22. Carman PC. Fluid flow through granular beds. *Transactions of the Institute of Chemical Engineers* 1937; **15**:150–166.
23. Mitchell JK. *Fundamentals of Soil Behavior*. (2nd edn). Wiley: New York, 1993.